

Article

Decentralised Active Power Control Strategy for Real-Time Power Balance in an Isolated Microgrid with an Energy Storage System and Diesel Generators

Hyeon-Jin Moon ¹, Young Jin Kim ^{2,*}, Jae Won Chang ¹ and Seung-Il Moon ¹

¹ Department of Electrical and Computer Engineering, Seoul National University, 1 Gwanak-ro, Seoul 08826, Korea; mhj7527@gmail.com (H.-J.M.); jwchang91@gmail.com (J.W.C.); moonsi@snu.ac.kr (S.-I.M.)

² Department of Electrical Engineering, Pohang University of Science and Technology (POSTECH), Pohang, Gyungbuk 37673, Korea

* Correspondence: powersys@postech.ac.kr; Tel.: +82-54-279-2368

Received: 8 December 2018; Accepted: 2 February 2019; Published: 6 February 2019



Abstract: Remote microgrids with battery energy storage systems (BESSs), diesel generators, and renewable energy sources (RESs) have recently received significant attention because of their improved power quality and remarkable capability of continuous power supply to loads. In this paper, a new proportional control method is proposed using frequency-bus-signaling to achieve real-time power balance continuously under an abnormal condition of short-term power shortage in a remote microgrid. Specifically, in the proposed method, the frequency generated by the grid-forming BESS is used as a global signal and, based on the signal, a diesel generator is then controlled indirectly. The frequency is controlled to be proportional to the AC voltage deviation of the grid-forming BESS to detect sudden power shortages and share active power with other generators. Unlike a conventional constant-voltage constant-frequency (CVCF) control method, the proposed method can be widely applied to optimise the use of distributed energy resources (DERs), while maintaining microgrid voltages within an allowable range, particularly when active power balance cannot be achieved only using CVCF control. For case studies, a comprehensive model of an isolated microgrid is developed using real data. Simulation results are obtained using MATLAB/Simulink to verify the effectiveness of the proposed method in improving primary active power control in the microgrid.

Keywords: microgrid; energy storage system; distributed generator; frequency control; active power control; autonomous control; droop control; frequency bus-signaling

1. Introduction

The penetration of renewable energy sources (RESs) such as photovoltaics (PVs) and wind turbines (WTs) is steadily increasing due to enhanced price competitiveness and the requirement of sustainable energy mixes. However, intermittent power outputs of RESs are detrimental to frequency and voltage stabilities, particularly in a small power system: e.g., a microgrid possessing a low moment of inertia [1,2]. A microgrid is an integrated platform that consists of power generation units, energy storage systems (ESSs), and demand response (DR) resources, whose operations are managed in a localised manner. The platform can be equipped with various functions for local power and energy management [3] under both grid-connected and islanded operating modes. In islanded mode, power demand and supply should be always balanced by itself using such distributed energy resources (DERs) in the system.

Electric utilities have technical difficulties in connecting remote microgrids on small oceanic islands to a bulk power grid on the mainland. It is also cost-ineffective and, therefore, electric

power supply in these remote microgrids relies primarily on diesel generators located in the area. Power outputs from diesel generators can be adjusted in real time to achieve power balance and hence maintain frequency and voltage stabilities [4]. However, heavy reliance on conventional diesel generators can lead to the following problems:

- Degradation of power quality and reliability due to the low inertia moment and constant-speed control scheme of diesel engines [2,5].
- High generation cost and volatility due to fuel import and transportation [6,7].
- Environmental issues such as carbon emission and air/noise pollution [6–9].

The development of ESS technologies has enabled RESs to become an attractive option for supplying electricity in such remote microgrids [4,6]. This is mainly because inverter-interfaced ESSs can alleviate the effects of intermittency of RESs on the operating stability of an isolated microgrid [10], given large penetration of RESs. Specifically, a battery energy storage system (BESS) can operate as a grid-forming unit that primarily regulates microgrid voltage and frequency [11–13]. A microgrid operator can access the BESS inverter and control the charging or discharging power of the battery within a short period of time [13], while maintaining state of charge (SOC) within an acceptable range for device protection and continuous use for other microgrid operating schemes (e.g., economic dispatch) [11–15]. Other DERs can be considered as grid-feeding units that follow the reference signals of active and reactive power.

In previous studies [14–39], grid-forming BESSs were widely used for the operation of isolated microgrids. In [16], a constant-voltage constant-frequency (CVCF) control scheme was adopted for BESSs to maintain frequency and voltages at their rated levels and consequently achieve real-time power balance in an isolated microgrid. In [17–26], the control scheme was practically applied to isolated microgrids in remote islands (including several islands in South Korea) mainly due to simple implementation and low fluctuations in grid frequency and voltages. However, the scheme requires large capacities of battery and inverters to achieve the real-time power balance under the condition on large variations in load demand and RES power outputs. To mitigate the operational burden of the BESS, centralised control methods were discussed in [15,27–30] for secondary active power regulation using real-time communications systems. Although such centralised methods are effective in optimal and robust operation of microgrids, they are vulnerable to a single point of failure (i.e., a part of a system that prevents the normal operation of the entire system if it fails). This degrades the reliability of isolated microgrids [31,32].

This challenge was considered in [33–37]; decentralised and autonomous control schemes were adopted as alternative options in which device-level controllers of individual units operate using local measurements of microgrid frequency. Unlike the centralised control schemes, the decentralised schemes allow the microgrid to operate continuously with the plug-and-play feature [31] (even under the condition of the single-point failure) and hence improve the operational reliability of the microgrid. In the decentralised schemes, droop controllers were commonly used to achieve power sharing among DERs. For example, power-and-frequency droop controllers were discussed to coordinate RESs and ESSs in [33,34] or adjust terminal voltage of the battery bank in [14]. In [34], the decentralised active power management scheme of multiple BESSs and distributed generators (DGs) was developed using multi-segment power-frequency characteristic curves. However, droop control has an inherent limitation that causes continuous fluctuations in microgrid frequency during the process of real-time power balancing [35]. Therefore, in [25,36–38], bus-signaling methods (rather than droop control methods) were exploited to induce the mode-change of DERs using the frequency and voltage control signals of BESSs while maintaining the SOC levels within allowable ranges. In [37], both droop control and bus-signaling methods were integrated with the CVCF controller mainly to maintain the SOC value of the BESS at a pre-determined level. However, these methods mainly focused on the battery energy management rather than the real-time power management in the microgrid.

Based on these observations, this paper proposes a new decentralised scheme integrated with frequency-bus-signaling and droop control based on a single-master and multiple-slaves configuration mainly to improve power sharing and real-time power balancing under the condition where serious disturbances occur in an isolated microgrid. In coordination with the CVCF controller, the proposed scheme enables the BESS to control the microgrid frequency in response to the change in AC voltages, given that unexpected voltage changes at the grid-forming converter bus indicate the instantaneous active power imbalance in the microgrid [39]. The proposed decentralised scheme enables autonomous power management in the microgrid via the coordination of the BESS with other DERs (particularly for the condition of lack of power generation), minimising the frequency and voltage deviations. Simulation case studies are performed using detailed models of an isolated microgrid in South Korea implemented with real parameters. Case study results demonstrate the effectiveness of the proposed control scheme in [40] mainly from the aspects of the following key advantages:

- Given extreme disturbances (such as a trip of the DGs), real-time power balance in an isolated microgrid is achieved without using communication systems.
- It has a simple structure and hence can be easily implemented in the outer control loop of the grid-forming BESS while ensuring the normal operations of inner control loops and, consequently, the device-level stability.
- Only the CVCF control is activated under normal operating conditions, minimising the fluctuation of microgrid frequency and active power of other DGs.

It needs to be noted that this paper is an extended version of our previous paper [40], including further improvements over [40] that can be summarized as follows:

- Performing additional literature review and further clarification between the proposed control scheme and conventional methods discussed in [11–42].
- Supplementing detailed explanations on the proposed control method and its simulation results, as well as the test bed with respect to load models and diesel generators
- Performing simulation case studies with consideration of practical microgrid components such as dead-bands and maximum/minimum limiters.

2. System Description

2.1. Geocha Island Microgrid

Figure 1 shows Geocha Island, located on the southwestern coast of South Korea. It consists of the West- and East-Geocha Islands which are 3.23 km² and 2.29 km² in area, respectively.



Figure 1. Isolated microgrid on Geocha Island, South Korea.

In 2017, a remote, isolated microgrid was established by the Korea Electric Power Corporation (KEPCO), mainly because of the difficulty in laying electrical power lines between the island and the Korean mainland. As shown in Figure 1, the main electrical facilities and power lines have no connection to the main grid. The west and east islands are connected via a 6.9-kV distribution line, which is characterised by a floating delta connection [26].

Figure 2 shows a schematic diagram of the microgrid configuration. The upper and lower parts represent the distribution lines in the west and east islands, respectively. The microgrid includes a 250-kW, 500-kWh BESS, a 100-kW PV, a 100-kW WT, and three 150-kW diesel generators. In the isolated microgrid, an energy management system (EMS) has been implemented to monitor the real-time operation of the DERs. Specifically, the PV and WT operate using maximum-power point tracking (MPPT) algorithms to maximise their power outputs for variations in solar insolation and wind speed, respectively [43,44]. In addition to the PV and WT, the diesel generators supply power as a grid-feeding unit to meet the load demand and maintain the SOC levels of the BESS within an acceptable range. The BESS operates as a grid-forming unit in charge of providing the primary reserve to the microgrid. While acting as a grid-forming unit, the BESS regulates the voltage and frequency of the isolated microgrid at the rated values using a CVCF control scheme to maintain the active and reactive power balance in a primary control level.

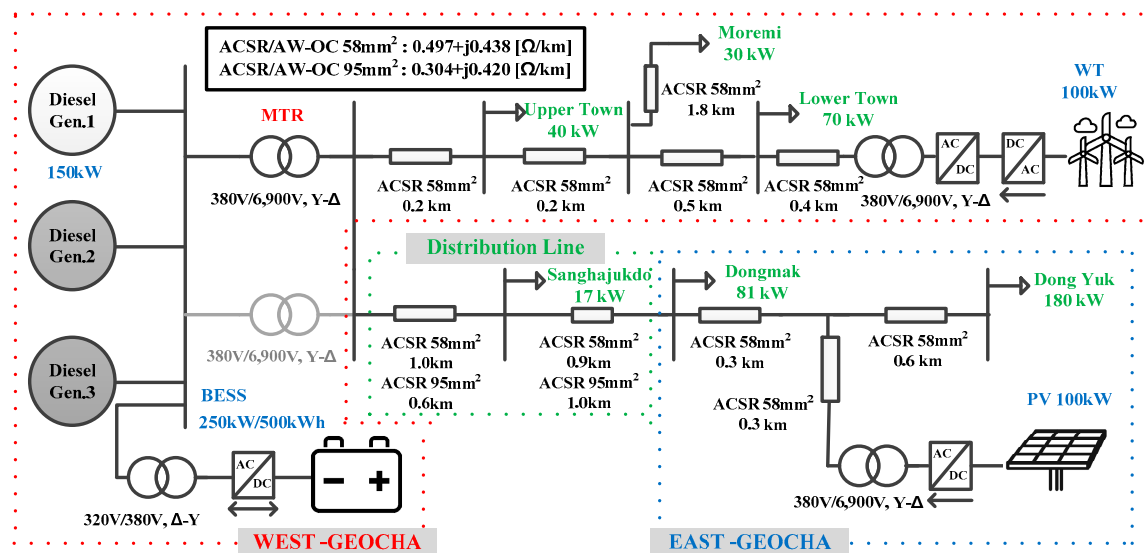


Figure 2. Schematic diagram of Geocha Island microgrid.

2.2. Grid-Forming BESS

A grid-forming BESS regulates the AC bus voltage and frequency by balancing power supply and demand in an isolated microgrid. The BESS consists of a battery pack, an LC filter, an inverter, and a transformer (see Figure 3). It operates as an AC voltage source and determines the levels of microgrid frequency and voltage by using conventional nested voltage and current control loops that operate on the dq reference frame. The BESS detects the instantaneous power imbalance by measuring the capacitor voltage V_c and recovers it to the reference value with the internal voltage and current controller. In the conventional CVCF control scheme, the dq voltage and frequency references are set to their rated values: i.e., $V_d^* = 1$ pu, $V_q^* = 0$, and $f^* = 1$ pu. The active and reactive power outputs of the BESS are indirectly controlled to maintain the bus voltage to the rated value. In this study, the frequency reference is calculated to share active power with other DERs by the proposed voltage-frequency proportional controller (VFPC), based on the level of voltage deviation, as explained in Section 3 in detail.

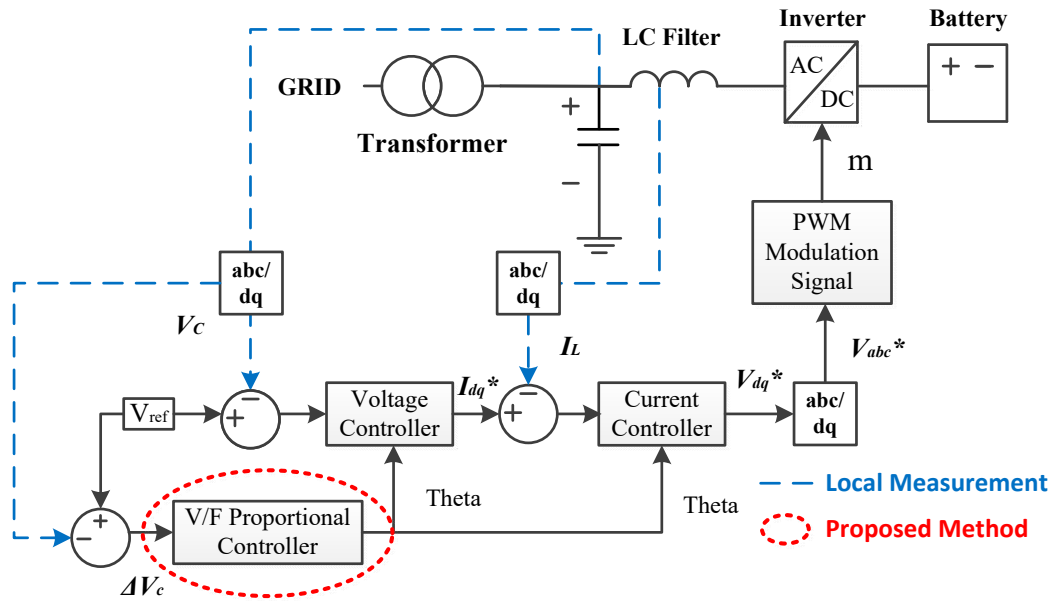


Figure 3. A schematic diagram of the grid-forming BESS and its device-level controllers.

2.3. Diesel Generator

Droop control is widely applied to improve the grid operational performance, stability, and reliability. It is based only on local measurements and allows generators in the system to operate autonomously. A droop control scheme is adopted such that the diesel generators can share active power with the BESS for real-time power balance. The droop control of active power can be expressed as:

$$f_{ref} = f_{set} - K_p(P_m - P_{set}), \quad (1)$$

where f_{ref} is the reference frequency of a generator and f_{set} and P_{set} are the presets of microgrid frequency and active power determined by the microgrid operator, respectively. P_m is a measured value of active output power of a generator and K_p is a droop coefficient that can be determined considering the operating frequency range in a microgrid as:

$$K_p = \frac{a(f_{max} - f_{min})}{P_{nom}}, \quad (2)$$

where f_{max} and f_{min} are the maximum and minimum values of the grid frequency, respectively. Moreover, P_{nom} is the nominal active power of a generator and a is a constant for determining the droop coefficient.

Figure 4 shows a schematic diagram of the active power controller of the diesel generator. It includes an active power droop controller and a PI controller for time-delay dynamic models of a valve actuator, a diesel engine, and a synchronous machine. Note that the synchronous machine was modelled using the SI fundamental block in the MATLAB/Simulink. The parameters related to the controller are determined using those provided in [23]. The droop controller generates ω_{ref_di} and the PI controller is used to track the reference signal by comparing ω_{ref_di} and ω_{m_di} . Note that ω_{m_di} is the measured angular frequency of a diesel generator.

Similarly, the droop controller is widely used for reactive power control and consequently AC voltage control, as shown in Figure 5. It consists mainly of a reactive power droop controller, a PI controller, and a transfer function model of an exciter. The reactive power control can be represented using the reactive droop coefficient K_q as:

$$V_{ref} = V_{set} - K_q(Q_m - Q_{set}) \quad (3)$$

$$K_q = \frac{b(V_{max} - V_{min})}{Q_{nom}} \tag{4}$$

In Equation (3), V_{ref} is the reference value of the bus voltage of a diesel generator. The values of V_{set} and Q_{set} correspond to the preset values of bus voltage and reactive power, respectively. In addition, Q_m and Q_{nom} are the measured and nominal reactive powers of a generator. Moreover, V_{max} and V_{min} denote the maximum and minimum voltages of the system and b is a constant for determining the reactive power droop coefficient.

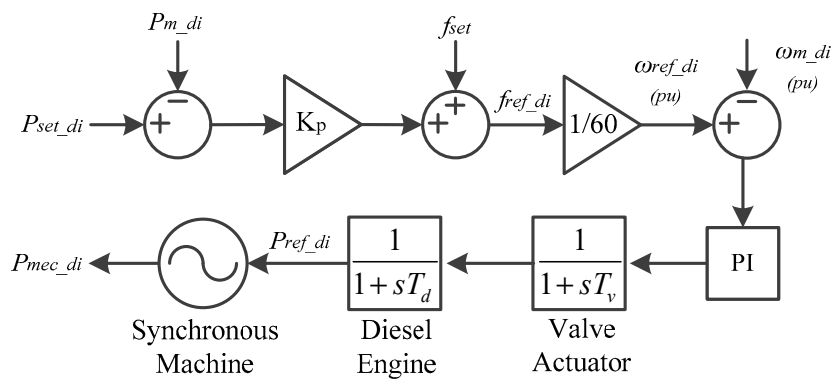


Figure 4. A schematic diagram for the active power controller of the diesel generator.

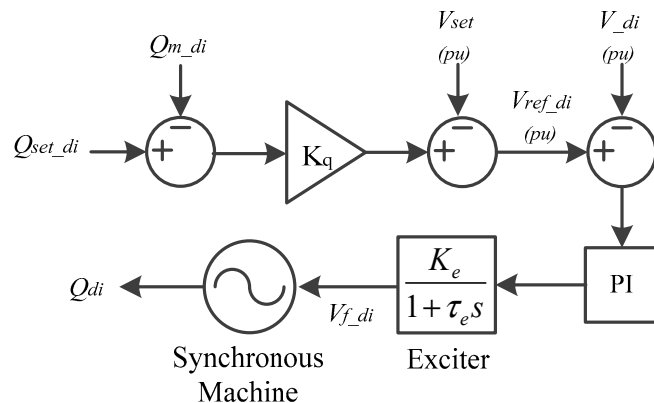


Figure 5. A schematic diagram for the reactive power controller of the diesel generator.

2.4. Basic Load Model

Load demand can be represented in terms of bus voltages [41] as:

$$P = P_0 \left(\frac{V}{V_0} \right)^{n_p} \tag{5}$$

$$Q = Q_0 \left(\frac{V}{V_0} \right)^{n_q} \tag{6}$$

where P_0 and Q_0 are active and reactive power demands at the rated operating voltage V_0 . In addition, P and Q are active and reactive power demands for actual bus voltage V . Furthermore, n_p and n_q are the exponents that vary depending on the inherent characteristics of the load devices. These exponents essentially represent the sensitivities of the load demands with respect to the bus voltage V : i.e., $\partial P/\partial V$ and $\partial Q/\partial V$ at $V = V_0$. Equations (1) and (2) can then be represented equivalently using a ZIP model [41] that has been commonly adopted in power system analysis as:

$$P = P_0 \left[Z_p \left(\frac{V}{V_0} \right)^2 + I_p \left(\frac{V}{V_0} \right) + P_p \right] \tag{7}$$

$$Z_p + I_p + P_p = 1 \quad (8)$$

$$Q = Q_0 \left[Z_q \left(\frac{V}{V_0} \right)^2 + I_q \left(\frac{V}{V_0} \right) + P_q \right] \quad (9)$$

$$Z_q + I_q + P_q = 1 \quad (10)$$

where Z_p , I_p , and P_p are the constant impedance, constant current, and constant power coefficients of active power demand, respectively. Similarly, Z_q , I_q , and Q_q are the ZIP coefficients of reactive power demand. The sum of the three coefficients must be equal to one, as shown in Equations (8) and (10), to meet the rated operating condition. Note that in this paper, we focus on the active power management in an isolated microgrid. In [42], the average value of n_p was known to be between 1.1 and 1.7. In isolated microgrids, n_p is expected to be larger due to the high proportion of resistive loads such as heating and lighting [42]. Therefore, n_p has been set to 2. This assumed that the isolated microgrid only includes constant impedance loads (i.e., $Z_p = 1$, $I_p = 0$, and $P_p = 0$).

2.5. Active Power Balance Equation in an Isolated Microgrid with CVCF Control

Under the normal operating condition where the grid-forming BESS has sufficient power reserve to cover the active power change of a system, the active power balance can be satisfied as:

$$\Delta P_{BESS} = \Delta P_{Load} + \Delta P_{Loss} - \Delta P_{DG} \quad (11)$$

where ΔP_{BESS} and ΔP_{DG} are the variations in the active power outputs of the grid-forming BESS and the DGs, respectively. ΔP_{Load} is the variation in the rated load demand and ΔP_{Loss} is the variation in active power losses in the microgrid. In contrast, the active power output of the BESS reaches its limit when the BESS does not have a sufficient power reserve. This limit can be estimated as:

$$\Delta P_{BESS_max} = V_c (I_{d_max} - I_{d_set}) \quad (12)$$

where ΔP_{BESS_max} is the maximum variation in the active power output of the BESS. In Equation (12), I_{d_max} and I_{d_set} are the maximum and preset values, respectively, of d -axis current. In this situation, the BESS cannot recover the voltage completely and, consequently, the load shedding is initiated by the bus voltage reduction to achieve the active power balance in the microgrid, as shown in Equations (13) and (14):

$$\Delta P_{BESS_max} = \Delta P_{Load} + \Delta P_{Loss} - \Delta P_{DG} - \Delta P_{Load_VR} \quad (13)$$

$$\Delta P_{Load_VR} = \sum \left[P_{Load_i0} \left\{ 1 - \left(\frac{V_i}{V_0} \right)^{n_{pi}} \right\} \right] \quad (14)$$

In Equation (14), ΔP_{Load_VR} is a decrease in the total load demand at under-voltage buses. As shown in Equation (14), the value of n_{pi} significantly affects the value of V_i at which the power balance in Equation (13) is satisfied. The smaller n_{pi} , the smaller V_i that is required to induce the enough reduction of the load demand, causing the degradation of voltage stability and even voltage collapse. This implies that for the microgrid with less voltage-dependent loads, the proposed VFPC becomes more effective in alleviating the power shortage and consequently mitigate the voltage reduction. Moreover, with less voltage-dependent loads, the proposed VFPC is capable of adjusting the frequency more successfully by inducing active participations of other diesel generators in the real-time frequency regulation via their P - f droop controllers.

3. Proposed Control Method

The IEEE standard recommends that the bus voltages should be regulated within 88–110% of the rated value for the normal operating condition [45]. The CVCF controller, discussed in Section 2, is effective in maintaining the voltages within the acceptable range particularly when the grid-forming

BESS operates with sufficient primary reserve. Otherwise, a cooperative control scheme of the CVCF controller of the BESS and the local controllers of other DGs needs to be implemented to exploit the additional primary reserve capacities of the DGs for the reliable operation of the isolated microgrid. The proposed cooperative control scheme aims at the active power sharing in an isolated microgrid when active power balance cannot be achieved solely by the CVCF controller of the grid-forming BESS. Figure 6 shows the flow chart of the proposed method for the decentralised active power control. In the proposed method, the BESS operating with the CVCF controller detects insufficient active power supply in the microgrid by measuring the input voltage of the AC bus where the BESS is connected. It then controls the frequency proportional to the bus voltage deviation from the nominal voltage. Further details on each module in Figure 6 will be discussed in Sections 3.1 and 3.2.

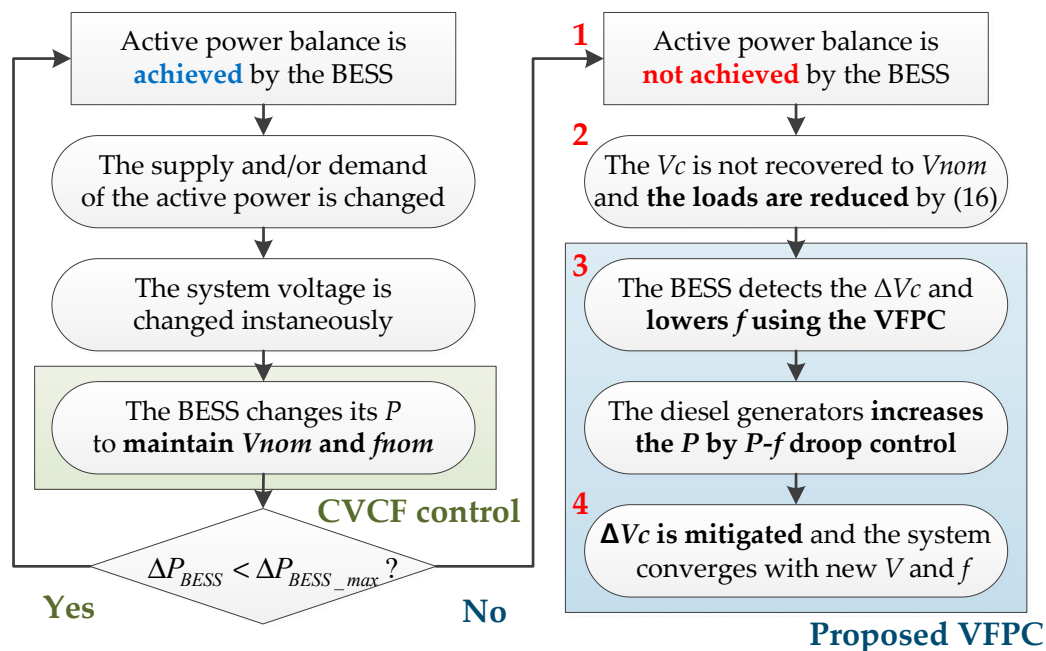


Figure 6. Flow chart of the proposed VFPC for the autonomous active power management at a primary control level.

In this paper, we focus on the coordinated, autonomous control scheme of the grid-forming BESS and the diesel generators via frequency-bus-signaling and droop control based on the single-master and multiple-slaves configuration. Note that for simplicity, the PV system and WT operate as independent current sources equipped with MPPT controllers without reactive power control. The proposed scheme also can be applied to a general microgrid including multiple BESS and diesel generators. In such microgrid, one BESS operates as a single-master unit that performs grid-forming control. The remaining BESSs and diesel generators operate as slave units using P - f droop control for power sharing. The operational burden on the master BESS will increase, causing the lack of active power reserve and hence frequent power shortages. This issue can be resolved using a multi-master droop control scheme (e.g., [13]). However, the scheme would cause continuous frequency deviations under the normal operating condition. Therefore, the microgrid operator needs to choose an appropriate configuration: i.e., the single-master and multiple-slaves or the multiple-masters and multiple-slaves. We leave the coordinated control of grid-forming master units in future work, while focusing on the development, analysis, and verification of the proposed control strategy based on the single-master-and-multiple-slaves configuration.

3.1. Frequency Control of BESS with VFPC

In this paper, a VFPC has been proposed to control the reference frequency of the grid-forming BESS, so that the primary active power reserve with the diesel generators is effectively exploited and shared in the microgrid under a power shortage condition. Specifically, in Figure 7, f_{nom} is the nominal frequency and f_{ref} is the reference frequency of the grid-forming BESS. The reference frequency is determined as:

$$f_{ref} = f_{nom} + K_v \Delta V_c \quad (15)$$

where ΔV_c is the variation in the AC voltage estimated by subtracting the actual AC voltage from the reference voltage of the BESS. The coefficient K_v denotes the proportional gain of the VFPC, which can be expressed as:

$$K_v = c \frac{f_{nom} - f_{min}}{V_{nom} - V_{min}} \quad (16)$$

where c is a constant to determine the V-f droop coefficient.

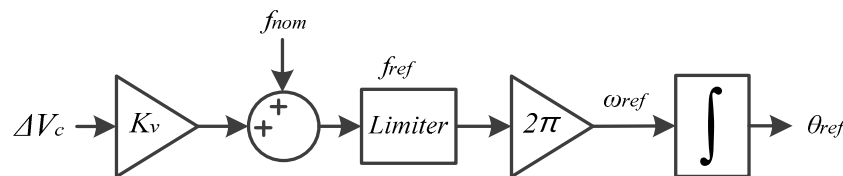


Figure 7. A schematic diagram of the V-f proportional controller for the grid-forming BESS.

In Figure 7, the limiter consists of dead-band, rate-limiter, and saturation blocks to operate only when the primary reserve of the grid-forming BESS is smaller than the magnitude of the load demand variation. The VFPC enables the BESS inverter to determine the system frequency for a decrease in the AC voltage, as shown in Equations (13) and (14), which is measured at the input port of the inverter. The diesel generators then measure the reduced system frequency and increase their active power outputs by conventional P - f droop controllers. Since the frequency is the same throughout the microgrid, the proposed frequency-bus-signaling method, discussed in Section 3.2, can achieve active power sharing in an autonomous manner.

3.2. Proposed Autonomous Active Power Management

The proposed VFPC of the grid-forming BESS is activated only if the active power balance cannot be achieved because of lack of the primary reserve of the BESS. Specifically, the capacitor voltage V_c is not fully recovered to V_{nom} when the BESS has insufficient the active power reserve and hence cannot compensate for all power imbalance in the microgrid. The BESS controls the frequency (i.e., f_{set} to f_{ref}) proportional to ΔV_c , as shown in Figure 8(Left), and then controls the diesel generators with active power droop curves (i.e., P_{set} to P_{ref}), as illustrated in Figure 8(Right). Considering the VFPC operation, a new power balance equation is represented as follows:

$$\Delta P_{BESS_max} = \Delta P_{Load} + \Delta P_{Loss} - \Delta P_{DG} - \Delta P_{Load_VR} - \Delta P_{Load_FR} - \Delta P_{DG_Droop} \quad (17)$$

$$\Delta P_{Load_FR} = K_{pf} \Delta f * P_{Load_0} \quad (18)$$

$$\Delta P_{DG_Droop} = P_m - P_{set} = -\frac{1}{K_p} (f_{ref} - f_{set}) = -\frac{K_v}{K_p} \Delta V_c \quad (19)$$

where ΔP_{Load_FR} is a variation in the load demand for the change in the microgrid frequency and ΔP_{DG_Droop} is the variation in the active power generation by droop control. In large-scale power systems, the load demand variation with respect to the frequency deviation can be characterized using the sensitivity coefficient K_{pf} in Equation (18), which varies for the range from 0 to 3.0 [41]. However, in this paper, the load demand is assumed to remain unchanged for the frequency deviation for simplicity.

This assumption is also valid because the reference frequency of the BESS is controlled to vary within a very small range, resulting in a slight variation in the microgrid frequency. For the VFPC, Equation (19) can then be derived from Equations (1) and (15). Equation (17) also can be expressed as:

$$\Delta P_{BESS_max} = \Delta P_{Load} + \Delta P_{Loss} - \Delta P_{DG} - \sum \left[P_{Load_i0} \left\{ 1 - \left(\frac{V_i}{V_0} \right)^{n_{pi}} \right\} \right] - K_{pf} \Delta f \times P_{Load_0} + \frac{K_v}{K_p} \Delta V_c \quad (20)$$

The integration of the VFPC with the CVCF controller of the grid-forming BESS enables additional primary reserve from the diesel generators to be exploited for real-time power balance in the microgrid via their active power droop control loops. In this way, autonomous active power management can be achieved for mitigating the active power shortage and the under-voltage, which often occur owing to the insufficient primary reserve of the BESS.

The proposed active power management strategy allows the grid-forming BESS to operate with the CVCF control under the normal condition where the BESS has sufficient primary reserve, so that the BESS can efficiently take charge of the primary reserve supply using its fast and accurate response characteristics. On the other hand, the frequency-bus-signaling method using the proposed VFPC is adopted for active power sharing with the diesel generators only under the abnormal condition where the BESS has the limited primary reserve. Consequently, the power sharing issue in the conventional CVCF control can be effectively resolved in the proposed strategy, minimising the microgrid frequency variations and the active power fluctuations of other droop-based DGs. The sequential operations of the VFPC can be summarised as follows:

1. The situation in which the remaining primary reserve of the BESS (ΔP_{BESS_max}) is not enough to cover the active power balance occurs due to a rapid increase in the net demand (e.g., sudden disconnection of a DG).
2. The overall bus voltage in the microgrid is reduced, inducing load reduction (ΔP_{load_VR}). This leads to the reduction of variations in the maximum power output of the BESS (see Equations (12) and (13)).
3. The BESS recognises the power shortage based on ΔV_c and reduces f_{ref} (see Equation (15)) by the VFPC. The diesel generator increases its active power with the P - f droop controller (see Equation (1)).
4. The participation of diesel generator, acting as a slave unit, enables the power shortage to be compensated for and consequently the microgrid voltages and load demand to be recovered. The reserve of the BESS is also procured and the microgrid starts operating with new levels of V and f (see Equation (20)).

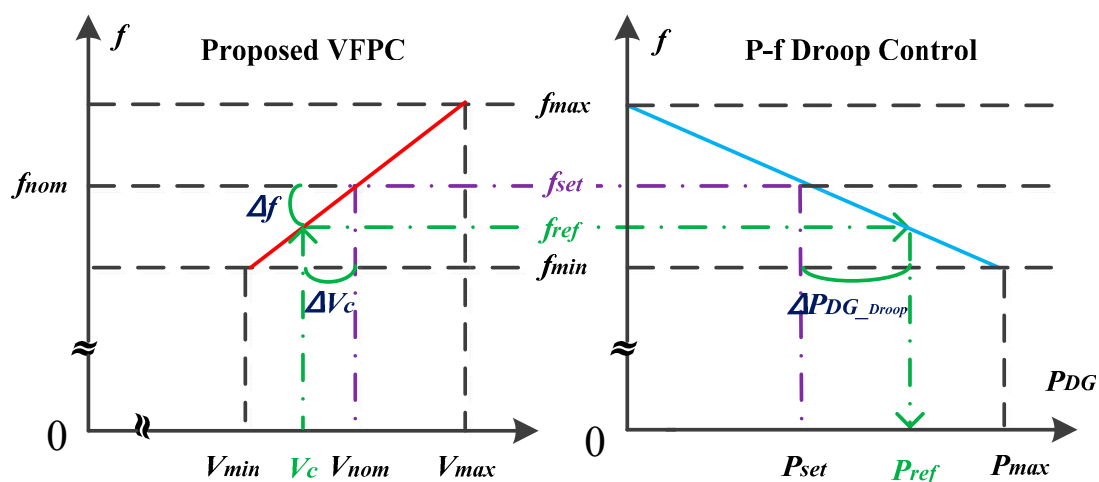


Figure 8. Comparison between (Left) the proposed control strategy (i.e., VFPC) of the grid-forming BESS and (Right) the conventional control strategy (i.e., droop controller) of the diesel generators.

are set to 238-kW, 90-kW, and 100-kW, respectively. The reactive power output of the diesel generator is set to 10-kVAr, and the reactive power reference of PV and WT are set to 0.

4.1. Simulation Results under the Normal Condition ($t < 9$ s)

Figure 10 shows the active power profiles of the grid-forming BESS, WT, PV, and diesel generator for Cases 1 and 2, respectively: (i) where only the conventional CVCF controller was adopted and (ii) where the proposed VFPC was integrated with the CVCF controller. The proposed VFPC was not activated by its limiter (see Figure 7) under the normal condition where the active power imbalance can be compensated for by the BESS. Therefore, Cases 1 and 2 have the same profiles of the active powers, voltages, frequencies, and load demand until $t < 9$ s, as shown in Figures 10–15. In both cases, the BESS maintained the active power balance and, consequently, the V_{BESS} and f_{BESS} at the rated values in the microgrid during $0 \text{ s} \leq t \leq 9 \text{ s}$. Specifically, during $0 \text{ s} \leq t \leq 3 \text{ s}$, the bus voltages at the WT and PV system increased to levels slightly higher than 1 pu. The voltages at the BESS were maintained at almost 1 pu, as shown in Figure 11. Figures 12–15 compare the profiles of the microgrid frequency at the main transformer, the reference frequency of the BESS, the total load demand, and the reactive power outputs in the microgrid for Cases 1 and 2. As shown in Figure 14, the actual load demand was observed at approximately 243 kW, which was greater than 238 kW at the rated bus voltages; the voltages at several load buses were higher than 1 pu, increasing the load demand due to the load-voltage dependency, as shown in Equation (14). In Figure 15, the reactive power outputs of the BESS and the diesel generator were maintained at an almost constant level due to the small variations in the reactive power loss and the feeder voltage.

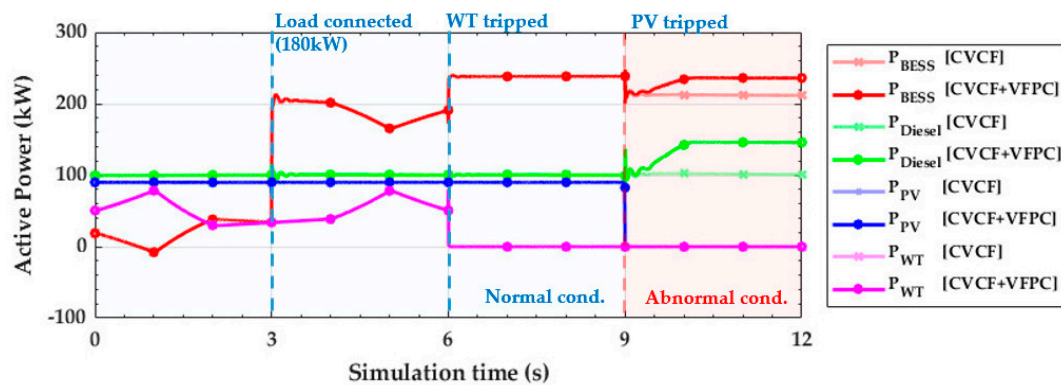


Figure 10. Profiles of the active power outputs of the BESS, WT, PV, and diesel generator.

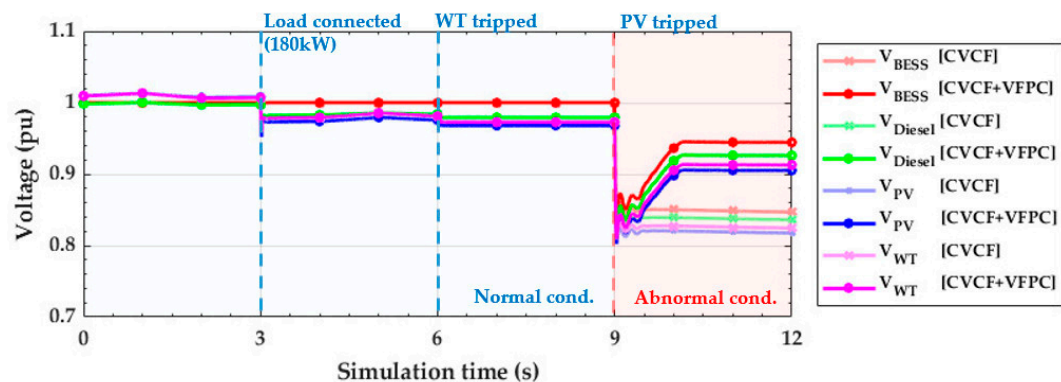


Figure 11. Profiles of the input voltages of the BESS, WT, PV, and diesel generator.

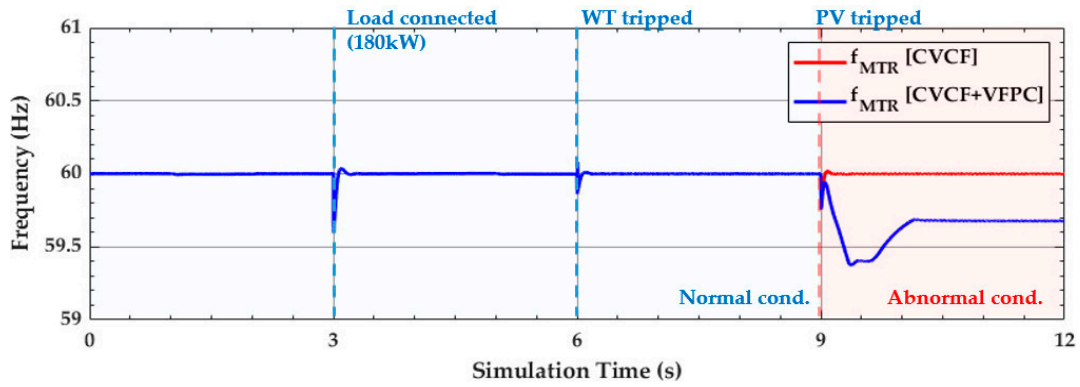


Figure 12. Comparison of the grid frequency profiles in the Geocha microgrid.

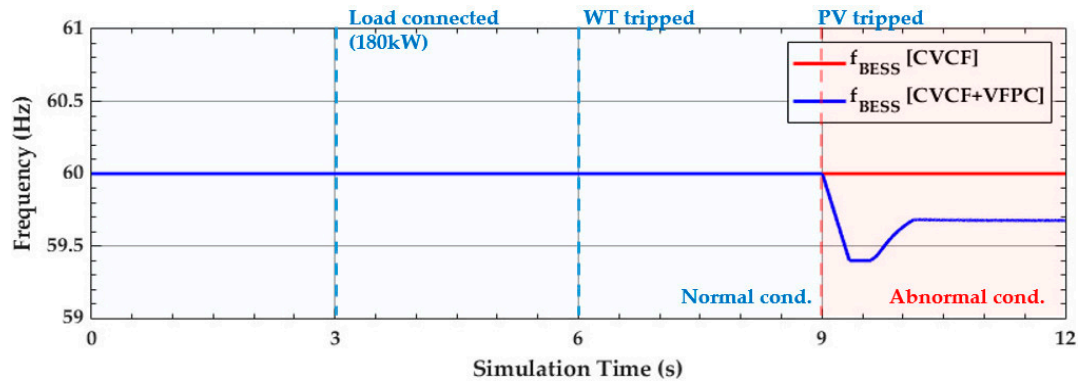


Figure 13. Comparison of the reference frequency profiles of the BESS in the Geocha microgrid.

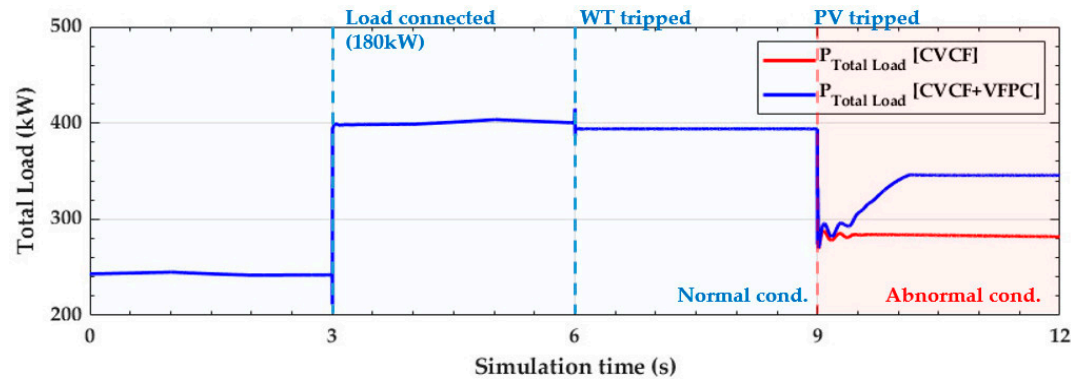


Figure 14. Comparison of the total load demand profiles in the Geocha microgrid.

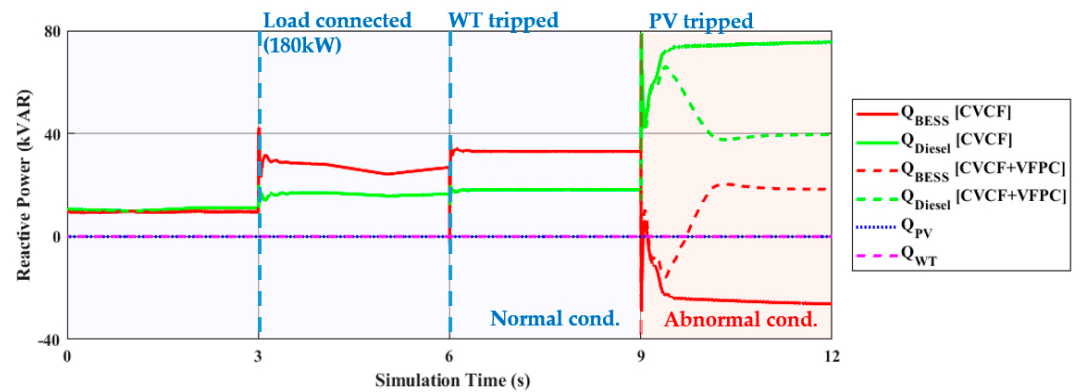


Figure 15. Profiles of the reactive power outputs of the BESS, WT, PV, and diesel generator.

When the 180-kW load was connected to the Dong-Yuk bus of the microgrid at $t = 3$ s, the nominal load demand increased from 238 kW to 418 kW in total. The microgrid voltage and frequency were then reduced instantaneously due to the large step increase in the load demand. The CVCF controller detected the voltage reduction and adjusted the output power of the BESS quickly from 34 kW to 213 kW, so as to maintain the power balance and the input voltage at the rated value. Meanwhile, the active power of the diesel generator fluctuated due to the frequency deviation during a short period of time. Figure 10 shows that the CVCF controller enabled the battery to respond to a large step-wise increase in the load demand within a short time period and maintain the real-time power balance in the microgrid. As shown in Figure 11, the small voltage drops were detected for the WT, PV system, and the diesel generator because of the increase in the power flowing along the distribution feeders connected from the west island to the east island. This increased active and reactive power losses on the substation transformers and in the distribution lines. The reactive power output of the BESS increased due to the increase in the reactive power loss in the microgrid, and the diesel generator then increased its reactive power output via the Q - V droop controller. During the period of $3 \text{ s} \leq t \leq 6 \text{ s}$, as shown in Figures 11 and 14, the actual load demand increased about from 398 kW to 403 kW and the bus voltage was reduced about from 0.967 pu to 0.986 pu.

At $t = 6$ s, the WT was tripped from the distribution feeder. The active power of the BESS then increased to maintain the power balance via the CVCF control, causing a further drop in the voltage at the buses of other DERs owing to the increase in the power flow from the substation. The total load demand then decreased owing to the additional voltage drops at the load buses. Meanwhile, other DERs retain their active power because the BESS was solely responsible for maintaining the active power balance at the primary control level. The active power output of the BESS increased from 190 kW to approximately 238 kW, as shown in Figure 10, which is similar to the rated active power output of 250 kW. The power balance could be achieved within a short period of time. However, the primary active power reserve was significantly reduced in the microgrid, affecting the power system reliability. The reactive power outputs of the BESS and the diesel generator slightly increased for the same reason as aforementioned.

4.2. Simulation Results under the Abnormal Conditions ($t \geq 9$ s)

When the PV system was tripped at $t = 9$ s, the active power reserve of the BESS could not afford the power balance. As a result, the bus voltages and hence the load demand decreased significantly, as shown in Figures 11 and 14. In the CVCF-only case, the diesel generator maintained its active power output as constants, because the microgrid frequency was maintained at f_{set} and the diesel generator could not detect the power imbalance with only its local measurement, as shown in Figures 10, 12 and 13. Consequently, the total load demand was significantly reduced to 282 kW, which is about 67% of the nominal demand, owing to the severe voltage reductions beyond the lower voltage limit of 0.9 pu: i.e., $V_{aBESS} = 0.847$ pu, $V_{aDiesel} = 0.836$ pu, $V_{aWT} = 0.824$ pu, and $V_{aPV} = 0.817$, as shown in Figures 11 and 14. Moreover, the reduction of the bus voltage at which the BESS is located also affected the active power output of the BESS, as shown in Equation (12). This is illustrated in Figure 10 where the active power output of the BESS is about 212 kW; it is lower than the rated active power. This further decreased the bus voltage. The large reduction of the feeder voltage caused the excessive compensation of the Q - V droop controller for the reactive power. Since the BESS is located close to the diesel generator in the remote microgrid, the excessive compensation could be immediately balanced using the BESS. It can be seen that the total reactive power supply and the reactive power loss increased mainly because of a further increase in the power flowing from the west island to the east island.

In contrast, the reference frequency of the BESS was reduced to 59.4 Hz due to the voltage drop (as shown in Figure 13) for Case 2 where the proposed VFPC was applied to the CVCF control in the BESS. The microgrid frequency was then reduced to 59.37 Hz and the diesel generator increased the active power to 145.9 kW via the droop control. The active power output of the BESS was also increased

to 236.1 kW, as shown in Equations (12) and (17), enabling the further recovery of the voltage drop. This coordinated control between the BESS and the diesel generator caused the microgrid voltage to rise by acquiring additional primary active power reserve in the microgrid. The compensation of the diesel generator for the reactive power was mitigated as the feeder voltage was gradually recovered. The microgrid frequency measured by a PLL was gradually restored to 59.68 Hz by increased power outputs of the diesel generator and the BESS. As shown in Figures 11 and 14, the proposed VFPC successfully mitigated the voltage drop ($V_{aBESS} = 0.944$ pu, $V_{aDiesel} = 0.926$ pu, $V_{aWT} = 0.913$ pu, and $V_{aPV} = 0.905$ pu) and the load reduction (about 72 kW, about 17% of the nominal demand).

4.3. Simulation Results with Less Voltage-Dependent Loads

In Case 3, the constant current load with the rated power of 81-kW was taken into consideration at the Dong-Mak bus (see Figure 2); n_p was reduced to approximately 1.65 at $t = 0$ s. After the constant impedance load of 180-kW was connected at the Dong-Yuk bus at $t = 3$ s, n_p increased from 1.65 to 1.81. The power shortage then led to larger decreases in the feeder voltages and consequently in the microgrid frequency during $t \geq 9$ s, compared to the original condition (i.e., Case 2) where only the constant impedance loads were considered. Figures 16–19 and Table 2 show that the lower n_p , the lower active power output of the BESS, further reducing the bus voltage, the frequency, and actual total load demand, particularly when the diesel generator failed to completely follow the command of the master BESS owing to the insufficient reserve capacity. In Figures 16–19, the full and dotted lines represent the cases of $n_p = 2$ and 1.81, respectively.

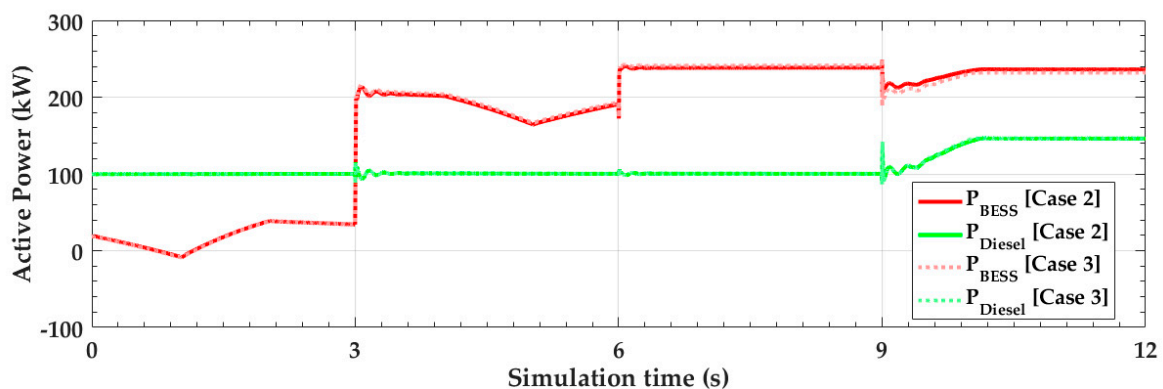


Figure 16. Profiles of the active power outputs of the BESS and diesel generator in Cases 2 and 3.

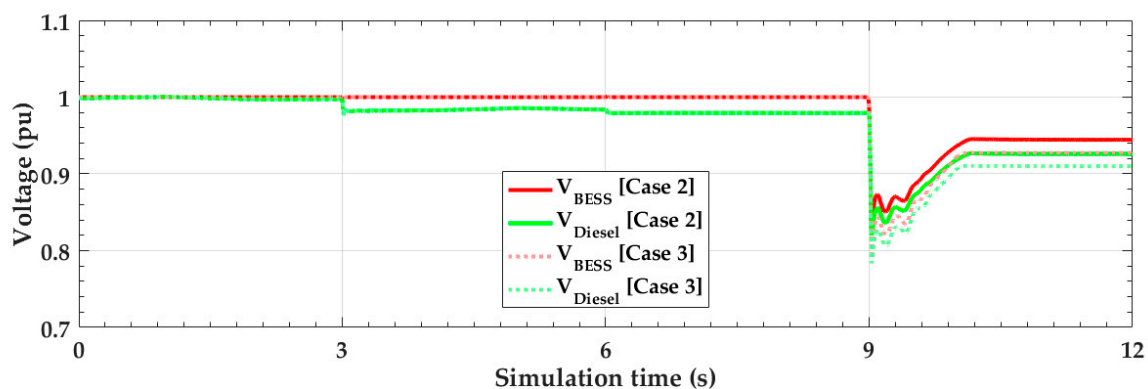


Figure 17. Profiles of the input voltages of the BESS and diesel generator in Cases 2 and 3.

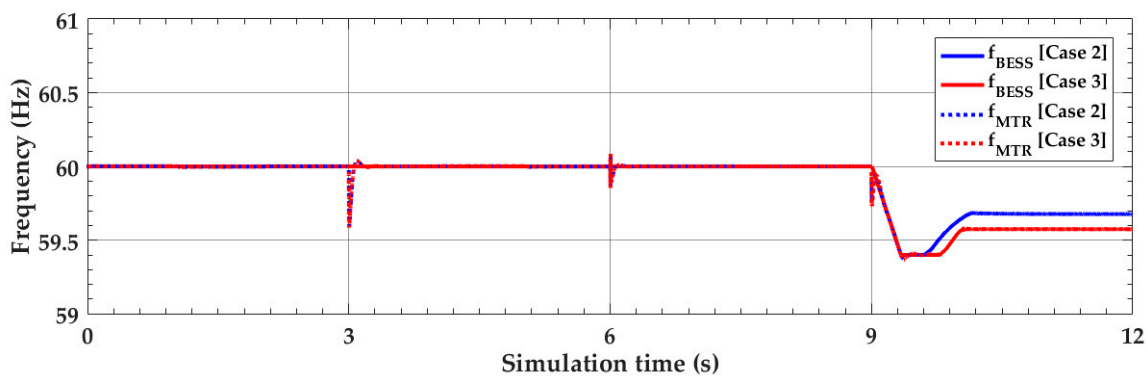


Figure 18. Comparisons of the frequency profiles at the main transformer and BESS in Cases 2 and 3.

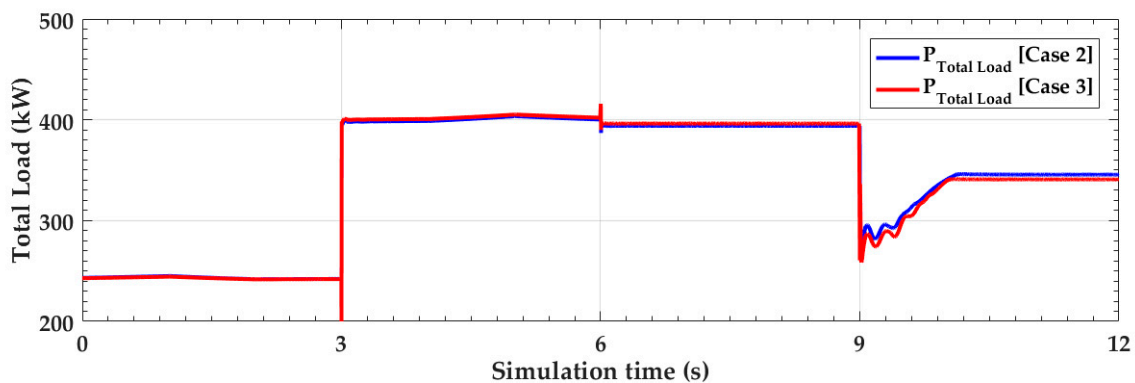


Figure 19. Comparisons of the total load demand profiles in the Geocha microgrid.

Table 2. Comparisons between the simulation results acquired for different load demand and compositions at $t = 12$ s.

	n_p	P_{load_0} (kW)	V_{aBESS} (pu)	$V_{aDiesel}$ (pu)	P_{BESS} (kW)	P_{Diesel} (kW)	P_{load} (kW)	f_{MTR} (Hz)
Case 2	2	418	0.944	0.926	236.1	145.9	345.6	59.68
Case 3	1.81	418	0.927	0.910	231.8	145.9	340.8	59.58
Case 2*	2	388	0.975	0.955	243.8	135.4	343.7	59.86
Case 4	1.56	388	0.969	0.949	242.3	143.7	350	59.83

In Cases 2* and 4, to simulate the less severe power shortage condition, the original condition was slightly modified to reduce Dong-Mak load from 81-kW to 51-kW. In addition, in Case 4, the 51-kW Dong-Mak load and the 40-kW Upper-Town load were modeled as constant power loads, reducing n_p to approximately 1.24 at $t = 0$ s. After the constant impedance load of 180-kW was connected at the Dong-Yuk bus at $t = 3$ s, increasing n_p from about 1.24 to 1.56. The power shortage occurred at $t = 9$ s in the microgrid, resulting in $n_p = 1.56$. It led to the bigger drop in the voltage and consequently caused the larger decrease in the frequency, in comparison to Case 2*. The maximum variation in the power output of the BESS was also reduced owing to the voltage drop, as shown in Equation (12). The diesel generator measured the frequency, which was further reduced, and increased its output power larger than those in Case 2*. This allowed the power shortage to be better compensated for and, consequently, the microgrid voltages and total load demand to be more recovered. Figures 20–23 then show that the lower n_p , the higher active power supply when the diesel generators had the sufficient reserve capacities and succeeded in following completely the command of the master BESS. This mitigated the reduction of actual load demand. Note the full and dotted lines represent the cases of $n_p = 2$ and 1.56, respectively. Table 2 shows that although the bus voltage, microgrid frequency, and BESS power output were reduced at $t = 12$ s for $n_p = 1.56$, the output power of the diesel generator and the total load demand were higher in Case 4 than those in Case 2*.

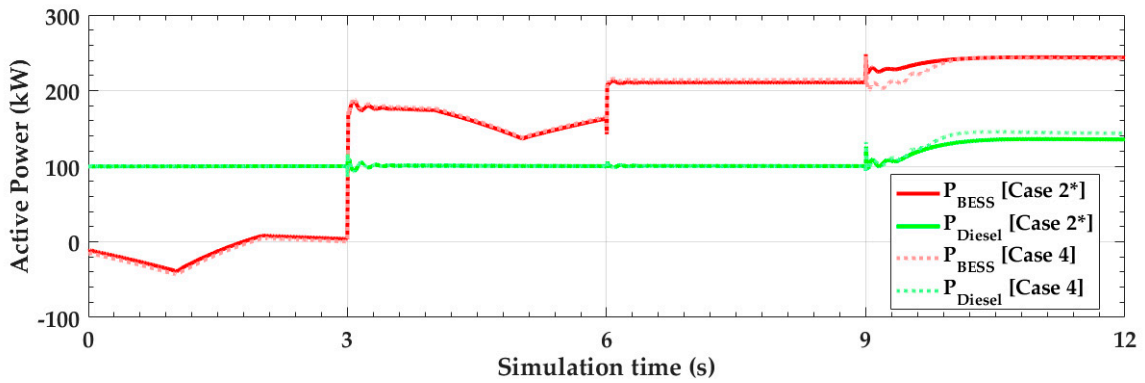


Figure 20. Profiles of the active power outputs of the BESS and diesel generator in Cases 2* and 4.

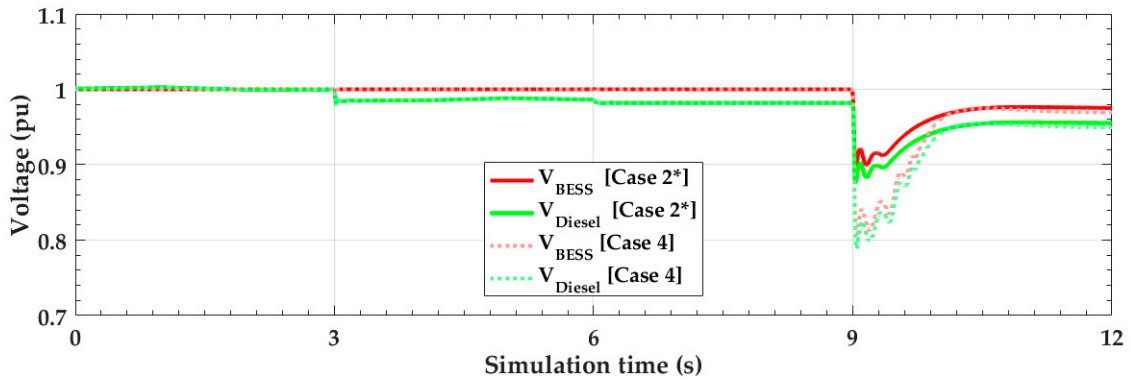


Figure 21. Profiles of the input voltages of the BESS and diesel generator in Cases 2* and 4.

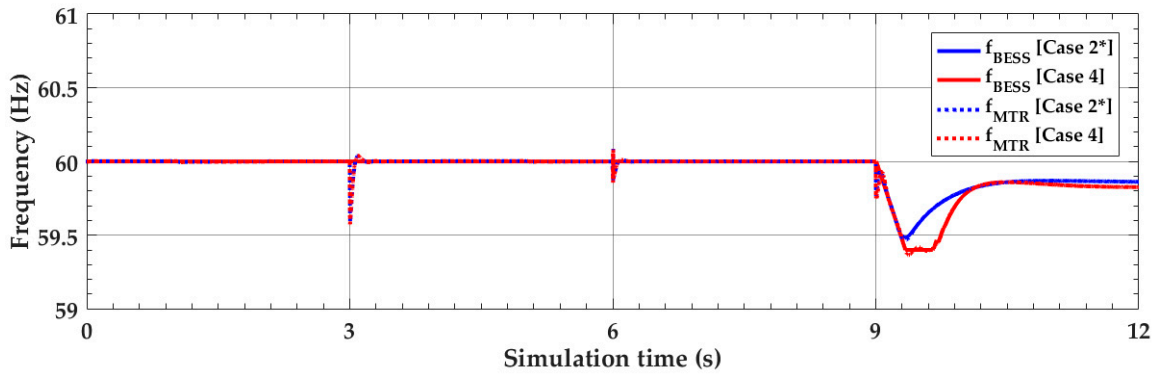


Figure 22. Comparisons of the frequency profiles at the MTR and BESS in Cases 2* and 4.

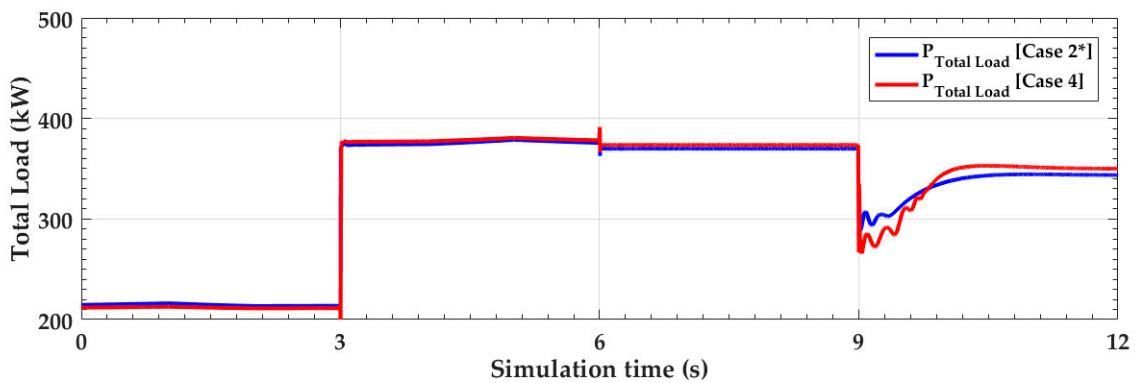


Figure 23. Comparisons of the total load demand profiles in Cases 2* and 4.

As shown in Cases 2–3 and 2*–4, the voltage drop becomes larger as n_p is reduced, particularly, under the power shortage condition. This implies that the proposed controller is more effective in alleviating the power shortage problem and voltage stability issue for a remote microgrid with less voltage-dependent load. The effect of the proposed controller becomes more evident when the slave units have sufficient reserve capacities.

4.4. Discussion

The CVCF control enables the grid-forming BESS to maintain the active power balance of the microgrid immediately by utilising the fast time response of the inverter. The grid-forming BESS is solely responsible for the active power balance in the microgrid at the primary level. Therefore, a cooperative method to induce the reserve provision of other DGs is required particularly when the limit of the BESS is reached. The simulation results in Section 4.2 show that when the primary active power reserve of the BESS is insufficient, and the load demand exceeds the power supply (after $t = 9$ s), the grid voltage is then greatly reduced overall, which reduces the load demand by the voltage-dependent characteristics of the loads. Furthermore, the active power reserve of the BESS is also reduced by the voltage drop at the BESS, exacerbating the active power imbalance in the microgrid.

The proposed VFPC operates only when the primary active power reserve of the microgrid is not enough by measuring the AC voltage of the BESS under the low-voltage condition. Under the normal condition (until $t = 9$ s in Section 4.1), the proposed method is able to reduce the microgrid frequency variation and the active power fluctuation, compared to the conventional f - P droop control method of the grid-forming BESS. In addition, this control method adjusts the frequency, which is proportional to the bus voltage of the BESS by the VFPC, to react to the diesel generator with active power droop control in the microgrid. Therefore, case studies results show that this method does not require any communication and can be easily applied with other conventional control methods such as CVCF and conventional droop control of other DERs.

Simulation results suggest that the conventional f - P droop control of the grid-forming BESS cannot operate properly when a large change in active power, such as a generator trip and step-load change, instantaneously occurs in the microgrid. These changes induce an instantaneous voltage drop, which reduces the maximum active power output of the grid-forming BESS. In this case, the conventional f - P controller receives the reduced active power of the BESS due to the voltage drop as an input signal, outputting the less reduced frequency. Then other DGs using P - f droop controllers cannot increase their active power outputs enough due to the frequency not being sufficiently reduced in the transient state.

It needs to be noted that in practice, it is likely for the microgrid operator to limit the reactive power supply to ensure the stable operation of the microgrid without significantly affecting the overall performance of the proposed active power management. In addition, due to the independent control of active and reactive power, the proposed method does not prevent the normal operation of the conventional reactive power controllers, mitigating the excessive compensation even for the case where the active power reserve is not sufficient.

5. Conclusions

In this paper, the VFPC has been proposed as an additional controller that can be easily integrated with the conventional CVCF controller of the BESS in the isolated microgrid. This effectively assists the microgrid operator to resolve the under-voltage problem owing to the limited reserve of the grid-forming BESS. This method uses the microgrid frequency as a global bus signal, enabling the indirect control of other DERs without communications systems. Moreover, the detailed simulation model was implemented in MATLAB/Simulink using actual system parameters to verify the effectiveness of the proposed active power management strategy. The simulation results show that the proposed VFPC method can mitigate the active power shortage and the bus voltage reduction using

the frequency-based operation of the DERs in the microgrid. From the simulation results, the main advantages of the proposed controller can be summarised as follows:

- The proposed VFPC can be easily applied to the existing CVCF controller of the grid-forming BESS and enables the coordinated control with other DERs that operate with conventional P - f droop controllers.
- The proposed VFPC can be activated based on the local measurement of its bus voltage, not active power, even when sudden and severe imbalance of active power takes place in the microgrid.
- The proposed controller is activated only during the period of active power imbalance. Unlike the conventional f - P droop method, the CVCF controller can still reduce the fluctuation of frequency and active power under the normal microgrid condition.

Author Contributions: Conceptualization, H.-J.M.; methodology, H.-J.M.; software, H.-J.M and J.W.C.; validation, H.-J.M., Y.J.K., J.W.C., and S.-I.M.; formal analysis, H.-J.M.; investigation, H.-J.M., Y.J.K.; resources, H.-J.M.; data curation, H.-J.M., J.W.C.; writing—original draft preparation, H.-J.M., Y.J.K., J.W.C., and S.-I.M.; writing—review and editing, H.-J.M., Y.J.K., J.W.C., and S.-I.M.; visualization, H.-J.M.; supervision, Y.J.K., S.-I.M.;

Acknowledgments: This work was supported by the Human Resources Development program of Korea Institute of Energy Technology Evaluation and Planning (KETEP) grant funded by Korea government Ministry of Trade, Industry and Energy (No. 20174030201540). This work was partly supported by the Korea Institute of Energy Technology Evaluation and Planning (KETEP) grant funded by the Korea government (MOTIE) (No. 70300037). This article is an extension of the work presented at ICEER2018 and published in Energy Procedia.

Conflicts of Interest: The authors declare no conflict of interest.

Abbreviations

Parameters of synchronous machine

Parameters	Symbols	Values	Units
Inertia coefficient	J	3.35	kg·m ²
Friction factor	F	0	N·m·s
Pole pairs	p	2	-
Stator resistance per phase	R_s	1.66×10^{-2}	Ω
Stator leakage inductance	L_l	1.68×10^{-4}	H
d -axis magnetizing inductance viewed from stator	L_{md}	5.86×10^{-3}	H
q -axis magnetizing inductance viewed from stator	L_{mq}	5.05×10^{-3}	H
Field resistance	R_f	5.25×10^{-3}	Ω
Field leakage inductance	L_{lfd}	6.82×10^{-4}	H
d -axis resistance of Damper	R_{kd}	1.53×10^{-1}	Ω
d -axis leakage inductance of Damper	L_{lkd}	3.40×10^{-3}	H
q -axis resistance of Damper	R_{kq1}	4.06×10^{-2}	H
q -axis leakage inductance of Damper	L_{lkq1}	6.08×10^{-4}	H
P gain of PI controller for active power control	K_{pp}	20	-
I gain of PI controller for active power control	K_{ip}	60	-
P gain of PI controller for reactive power control	K_{pq}	5	-
I gain of PI controller for reactive power control	K_{iq}	13	-

Parameters of synchronous machine controller

Parameters	Symbols	Values	Units
Time constant of diesel engine	T_d	0.5	s
Time constant of valve actuator	T_v	0.05	s
P - f droop coefficients of the diesel generator	K_p	4.0×10^{-6}	-
Amplification gain of the exciter	K_e	70	-
Time constant of the exciter	τ_e	2.0×10^{-3}	-
Q - V droop coefficient of the diesel generator	K_q	2.5×10^{-6}	-

P gain of PI controller for active power control	K_{pp}	20	-
I gain of PI controller for active power control	K_{ip}	60	-
P gain of PI controller for reactive power control	K_{pq}	5	-
I gain of PI controller for reactive power control	K_{iq}	13	-

References

- Teodorescu, R.; Liserre, M.; Rodriguez, P. *Grid Converters for Photovoltaic and Wind Power Systems*; John Wiley & Sons: West Sussex, UK, 2011; Volume 29.
- Jing, L.M.; Son, D.H.; Kang, S.H.; Nam, S.R. A Novel Protection Method for Single Line-to-Ground Faults in Ungrounded Low-Inertia Microgrids. *Energies* **2016**, *9*, 459. [[CrossRef](#)]
- Hatziargyriou, N. *Microgrids Architectures and Control*; Wiley, IEEE-Press: Chichester, UK, 2014; pp. XXI, 317. [[CrossRef](#)]
- Lu, X.N.; Wang, J.H. A Game Changer Electrifying remote communities by using isolated microgrids. *IEEE Electr. Mag.* **2017**, *5*, 56–63. [[CrossRef](#)]
- Lee, J.H.; Lee, S.H.; Sul, S.K. Variable-Speed Engine Generator with Supercapacitor: Isolated Power Generation System and Fuel Efficiency. *IEEE Trans. Ind. Appl.* **2009**, *45*, 2130–2135. [[CrossRef](#)]
- Neto, M.R.B.; Carvalho, P.C.M.; Carioca, J.O.B.; Canafistula, F.J.F. Biogas/photovoltaic hybrid power system for decentralized energy supply of rural areas. *Energy Policy* **2010**, *38*, 4497–4506. [[CrossRef](#)]
- Arent, D.; Barnett, J.; Mosey, G.; Wise, A. The potential of renewable energy to reduce the dependence of the state of Hawaii on oil. In Proceedings of the 42nd HICSS'09 Hawaii International Conference on System Sciences, Waikoloa, HI, USA, 5–8 January 2009; pp. 1–11.
- Tong, Z.M.; Zhang, K.M. The near-source impacts of diesel backup generators in urban environments. *Atmos. Environ.* **2015**, *109*, 262–271. [[CrossRef](#)]
- Uddin, M.N.; Rahman, M.A.; Sir, M. Reduce Generators Noise with Better Performance of a Diesel Generator Set using Modified Absorption Silencer. *Glob. J. Res. Eng.* **2016**, *XVI*. Available online: https://globaljournals.org/GJRE_Volume16/5-Reduce-Generators-Noise.pdf (accessed on 6 February 2019).
- Prull, D.S. *Design and Integration of an Isolated Microgrid with a High Penetration of Renewable Generation*; University of California: Berkeley, CA, USA, 2008.
- Green, T.C.; Prodanovic, M. Control of inverter-based micro-grids. *Electr. Power Syst. Res.* **2007**, *77*, 1204–1213. [[CrossRef](#)]
- Katiraei, F.; Iravani, R.; Hatziargyriou, N.; Dimeas, A. Microgrids management. *IEEE Power Energy Mag.* **2008**, *6*, 54–65. [[CrossRef](#)]
- Wang, X.F.; Guerrero, J.M.; Blaabjerg, F.; Chen, Z. A Review of Power Electronics Based Microgrids. *J. Power Electron.* **2012**, *12*, 181–192. [[CrossRef](#)]
- de Matos, J.; Silva, F.; Ribeiro, L. Power Control in AC Isolated Microgrids with Renewable Energy Sources and Energy Storage Systems. *IEEE Trans. Ind. Electron.* **2014**, *62*. [[CrossRef](#)]
- Miao, Z.X.; Xu, L.; Disfani, V.R.; Fan, L.L. An SOC-Based Battery Management System for Microgrids. *IEEE Trans. Smart Grid* **2014**, *5*, 966–973. [[CrossRef](#)]
- Bevrani, H.; François, B.; Ise, T. *Microgrid Dynamics and Control*; John Wiley & Sons: Hoboken, NJ, USA, 2017.
- Kim, H.; Bae, J.; Baek, S.; Nam, D.; Cho, H.; Chang, H.J. Comparative Analysis between the Government Micro-Grid Plan and Computer Simulation Results Based on Real Data: The Practical Case for a South Korean Island. *Sustainability* **2017**, *9*, 197. [[CrossRef](#)]
- Kim, S.-Y.; Mathews, J.A. Korea's Greening Strategy: The role of smart microgrids. *Asia-Pac. J.* **2016**, *14*, 6.
- Hwang, W.H.; Kim, S.K.; Lee, J.H.; Chae, W.K.; Lee, J.H.; Lee, H.J.; Kim, J.E. Autonomous Micro-grid Design for Supplying Electricity in Carbon-Free Island. *J. Electr. Eng. Technol.* **2014**, *9*, 1112–1118. [[CrossRef](#)]
- Chae, W.K.; Lee, H.J.; Won, J.N.; Park, J.S.; Kim, J.E. Design and Field Tests of an Inverted Based Remote MicroGrid on a Korean Island. *Energies* **2015**, *8*, 8193–8210. [[CrossRef](#)]
- Kim, S.-H.; Chung, I.-Y.; Lee, H.-J.; Chae, W.-K. Voltage and Frequency Control Method Using Battery Energy Storage System for a Stand-alone Microgrid. *Trans. Korean Inst. Electr. Eng.* **2015**, *64*, 1168–1179. [[CrossRef](#)]

22. Chae, W.K.; Won, J.N.; Lee, H.J.; Kim, J.E.; Kim, J. Comparative Analysis of Voltage Control in Battery Power Converters for Inverter-Based AC Microgrids. *Energies* **2016**, *9*, 596. [[CrossRef](#)]
23. Kim, Y.S.; Kim, E.S.; Moon, S.I. Frequency and Voltage Control Strategy of Standalone Microgrids with High Penetration of Intermittent Renewable Generation Systems. *IEEE Trans. Power Syst.* **2016**, *31*, 718–728. [[CrossRef](#)]
24. Kim, H.; Baek, S.; Choi, K.H.; Kim, D.; Lee, S.; Kim, D.; Chang, H.J. Comparative Analysis of On- and Off-Grid Electrification: The Case of Two South Korean Islands. *Sustainability-Basel* **2016**, *8*, 350. [[CrossRef](#)]
25. Moon, H.-J.; Chang, J.W.; Kim, E.-S.; Moon, S.-I. Frequency-based wireless control of distributed generators in an isolated microgrid: A case of Geocha Island in South Korea. In Proceedings of the 2017 52nd International Universities Power Engineering Conference (UPEC), Crete, Greece, 28–31 August 2017; pp. 1–6.
26. Won, J.; Chae, W.; Lee, H.; Park, J.; Sim, J.; Shin, C. Demonstration of remote microgrid system in Korean island. *CIREN-Open Access Proc. J.* **2017**, *2017*, 2212–2214. [[CrossRef](#)]
27. Belvedere, B.; Bianchi, M.; Borghetti, A.; Nucci, C.A.; Paolone, M.; Peretto, A. A Microcontroller-Based Power Management System for Standalone Microgrids with Hybrid Power Supply. *IEEE Trans. Sustain. Energy* **2012**, *3*, 422–431. [[CrossRef](#)]
28. Tan, K.T.; So, P.L.; Chu, Y.C.; Chen, M.Z.Q. Coordinated Control and Energy Management of Distributed Generation Inverters in a Microgrid. *IEEE Trans. Power Deliv.* **2013**, *28*, 704–713. [[CrossRef](#)]
29. Olivares, D.E.; Canizares, C.A.; Kazerani, M. A Centralized Energy Management System for Isolated Microgrids. *IEEE Trans. Smart Grid* **2014**, *5*, 1864–1875. [[CrossRef](#)]
30. Kaur, A.; Kaushal, J.; Basak, P. A review on microgrid central controller. *Renew. Sustain. Energy Rev.* **2016**, *55*, 338–345. [[CrossRef](#)]
31. Yazdani, M.; Mehrizi-Sani, A. Distributed Control Techniques in Microgrids. *IEEE Trans. Smart Grid* **2014**, *5*, 2901–2918. [[CrossRef](#)]
32. Abdelaziz, M.M.A.; Farag, H.E. An Enhanced Supervisory Control for Islanded Microgrid Systems. *IEEE Trans. Smart Grid* **2016**, *7*, 1941–1943. [[CrossRef](#)]
33. Wu, D.; Tang, F.; Dragicevic, T.; Vasquez, J.C.; Guerrero, J.M. A Control Architecture to Coordinate Renewable Energy Sources and Energy Storage Systems in Islanded Microgrids. *IEEE Trans. Smart Grid* **2015**, *6*, 1156–1166. [[CrossRef](#)]
34. Mahmood, H.; Jiang, J. Decentralized Power Management of Multiple PV, Battery, and Droop Units in an Islanded Microgrid. *IEEE Trans. Smart Grid* **2017**. [[CrossRef](#)]
35. Solanki, A.; Nasiri, A.; Bhavaraju, V.; Familant, Y.L.; Fu, Q. A New Framework for Microgrid Management: Virtual Droop Control. *IEEE Trans. Smart Grid* **2016**, *7*, 554–566. [[CrossRef](#)]
36. Schonbergerschonberger, J.; Duke, R.; Round, S.D. DC-bus signaling: A distributed control strategy for a hybrid renewable nanogrid. *IEEE Trans. Ind. Electron.* **2006**, *53*, 1453–1460. [[CrossRef](#)]
37. Wu, D.; Tang, F.; Dragicevic, T.; Vasquez, J.C.; Guerrero, J.M. Autonomous Active Power Control for Islanded AC Microgrids with Photovoltaic Generation and Energy Storage System. *IEEE Trans. Energy Convers.* **2014**, *29*, 882–892. [[CrossRef](#)]
38. Peyghami, S.; Mokhtari, H.; Blaabjerg, F. Autonomous Power Management in LVDC Microgrids Based on a Superimposed Frequency Droop. *IEEE Trans. Power Electr.* **2018**, *33*, 5341–5350. [[CrossRef](#)]
39. Mastromauro, R.A. Voltage control of a grid-forming converter for an AC microgrid: A real case study. In Proceedings of the 3rd Renewable Power Generation Conference (RPG 2014), Naples, Italy, 24–25 September 2014; pp. 1–6.
40. Moon, H.-J.; Chang, J.W.; Lee, S.-Y.; Moon, S.-I. Autonomous active power management in isolated microgrid based on proportional and droop control. *Energy Procedia* **2018**, *153*, 48–55. [[CrossRef](#)]
41. Kundur, P.; Balu, N.J.; Lauby, M.G. *Power System Stability and Control*; McGraw-Hill: New York, NY, USA, 1994; Volume XXIII, p. 1176.
42. Farrokhabadi, M.; Canizares, C.A.; Bhattacharya, K. Frequency Control in Isolated/Islanded Microgrids Through Voltage Regulation. *IEEE Trans. Smart Grid* **2017**, *8*, 1185–1194. [[CrossRef](#)]
43. Femia, N.; Petrone, G.; Spagnuolo, G.; Vitelli, M. Optimization of perturb and observe maximum power point tracking method. *IEEE Trans. Power Electr.* **2005**, *20*, 963–973. [[CrossRef](#)]

44. Abdullah, M.A.; Yatim, A.H.M.; Tan, C.W.A.; Saidur, R. A review of maximum power point tracking algorithms for wind energy systems. *Renew. Sustain. Energy Rev.* **2012**, *16*, 3220–3227. [[CrossRef](#)]
45. IEEE Guide for Design, Operation, and Integration of Distributed Resource Island Systems with Electric Power Systems. *IEEE Access* **2011**, 1–54. [[CrossRef](#)]



© 2019 by the authors. Licensee MDPI, Basel, Switzerland. This article is an open access article distributed under the terms and conditions of the Creative Commons Attribution (CC BY) license (<http://creativecommons.org/licenses/by/4.0/>).